JOURNAL OF CATALYSIS **176,** 536–544 (1998)
ARTICLE NO. CA982064

Chlorine-Induced Alterations in Oxidation State and CO Chemisorptive Properties of CeO_2-Supported Rh Catalysts

Dimitris I. Kondarides, Zhaolong Zhang, and Xenophon E. Verykios[1]

Department of Chemical Engineering, University of Patras, GR-26500 Patras, Greece

Received December 9, 1997; revised February 16, 1998; accepted February 18, 1998

The influence of residual chlorine species, originating from catalyst preparation procedures, on the carbon monoxide adsorption/desorption characteristics of Rh/CeO_2 catalysts and on the oxidation state of the supported rhodium particles is studied by FTIR and X-ray photoelectron spectroscopy. Depending on the preparation procedure and the experimental conditions, three rhodium species may coexist on the catalyst surface, i.e. Rh^0, Rh^+, and Rh^{3+}. The presence of Cl species is found to stabilize an amount of rhodium in the Rh^{3+} oxidation state and to alter significantly the CO adsorption and desorption behavior of the catalysts. The kinetic rate of approach to chemisorptive equilibrium as well as the relative population and the thermal stability of the adsorbed CO species at equilibrium are significantly affected by the presence of Cl on the catalyst surface.

1. INTRODUCTION

Rhodium- and ceria-containing catalysts have received particular attention in recent years mainly due to their use as components in three-way catalysts (TWC) for automotive emission control (1, 2). Ceria is added to automotive catalysts primarily for its oxygen storage capacity, which results from its ability to cycle between CeO_2 and CeO_{2-x}, thus operating as a regulator of the oxygen partial pressure over the catalysts. Furthermore, its reducibility may induce a certain type of metal–support interaction and generate favorable catalytic sites at the metal–support interface through the progressive depletion of oxygen-deficient phases with oxygen vacancies as predominant defects (3–5). The type of metal precursor used in the preparation of M/CeO_2 catalysts has been found to drastically influence the microstructure and catalytic properties of M/CeO_2 systems (6–9). This is due to the unique ability of ceria to retain chlorine species when prepared using a chloride-containing metal precursor, possibly due to the formation of a cerium oxychloride [$Ce^{(III)}OCl$] compound (6, 8, 10).

Rhodium, in addition to its importance for NO reduction in TWC systems (1, 2), has been extensively studied due to its unique catalytic properties which are associated with the relative importance of Rh^0 species compared with either Rh^+ or Rh^{3+}, i.e. in controlling selectivity for CO dissociation and CO insertion in the CO-hydrogenation reaction (11–15).

Qualitative information concerning the assignment of the oxidation state of rhodium species can be obtained employing infrared vibrational spectroscopy of adsorbed CO, while quantification is more straightforward with the use of XPS. In this regard, several studies employing XPS have been conducted to identify the oxidation state of rhodium particles supported on several carriers (15–20) under various experimental conditions. Concerning infrared studies of the CO/Rh system, much work has been done on rhodium particles supported on several oxides (15, 20–25) including CeO_2 (9, 26).

Yang and Garland (21) were the first who determined three types of carbonyl species following CO adsorption on Rh/Al_2O_3, i.e. gem-dicarbonyl [$Rh(CO)_2$], linear [Rh_x-CO], and bridged [Rh_2-CO] species. In an extensive investigation of the $CO/Rh/Al_2O_3$ system, Rice *et al.* (22) found eight different CO/Rh species, depending on the metal loading, the preparation method and the experimental conditions employed. The formation of the gem-dicarbonyl species observed upon CO adsorption on dispersed rhodium crystallites is usually attributed to disruption of rhodium particles and oxidation to Rh^+ by surface hydroxyl groups (27, 28) and/or to dissociation of CO followed by oxidation of Rh^0 with adsorbed oxygen (12, 29). At elevated temperatures, the disruption process is reversed and CO adsorption leads to the reductive agglomeration of Rh^+ species (28, 30).

The effect of residual chlorine on the chemisorptive properties of Rh/CeO_2 catalysts has been examined in a previous study in this laboratory employing XPS and TPD-MS techniques (31). It was found that Rh/CeO_2 catalysts prepared from $RhCl_3 \cdot 3H_2O$ contain a significant amount of chlorine species (7 at% to the depth probed by XPS) after reduction with hydrogen at 300°C, which induces significant changes to the oxidation state of cerium. The presence of residual chlorine resulted in a suppression of the capacity of the

[1] E-mail address: verykios@iceht.forth.gr.

0021-9517/98 $25.00

catalyst towards CO and H_2 adsorption and in changes in the relative population of the adsorbed species. Furthermore, a strongly adsorbed CO species, which was not observed over Cl-free Rh/CeO_2, was found to exist on the Cl-containing surface following CO adsorption in the temperature range of 25 to 300°C.

In the present work, a detailed FTIR and XPS study of CO adsorption/desorption behavior was conducted over 0.5% Rh/CeO_2 catalysts prepared with either $RhCl_3 \cdot 3H_2O$ or $Rh(NO_3)_3$ as metal precursors. The aim of this work is to assign the origin of the additional adsorbed CO species indicated in our previous study (31) and to study the oxidation state of rhodium particles supported on Cl-free and Cl-containing samples.

2. EXPERIMENTAL

Catalyst preparation. Two 0.5 wt% Rh/CeO_2 catalysts were prepared using $RhCl_3 \cdot 3H_2O$ or $Rh(NO_3)_3$ as metal precursors, employing the incipient wetness impregnation method, following the procedure described earlier (31). Weighed amounts of Rh metal precursor were dissolved in distilled water at 25°C, while an appropriate amount of the carrier (Cerium IV oxide powder 99.9%, Alfa, surface area: 3.6 m^2/g) was added to the solution under continuous stirring. The suspension was heated at 80°C to evaporate the water and the remaining slurry was dried in an oven at 110°C for 24 h. The solid residue was finally treated with hydrogen at 300°C for 2 h. The catalyst prepared using $RhCl_3 \cdot 3H_2O$ (Cl-containing) is designated as Rh/CeO_2(Cl) and the one prepared using $Rh(NO_3)$ (Cl-free) is designated as Rh/CeO_2(N).

XPS experiments. XPS experiments were carried out in a SPECS LHS 10 spectrometer employing the Mg k_α (1253.6 eV) exciting radiation at 157.5 W, with the analyser in the pass-energy mode, at a pass energy of 36 eV. All spectra were acquired at 25°C and a minimum background pressure of less than 5×10^{-9} mbar. Hydrogen and CO treatment was conducted in the introduction chamber of the apparatus where the sample can be treated with gases at atmospheric pressure and elevated temperature (31). Pretreatment of the samples included *in situ* reduction with hydrogen at 300°C for 30 min at atmospheric pressure, cooling to room temperature under hydrogen flow and evacuation to 10^{-3} mbar. Preliminary experiments showed that there is no difference in the XPS spectra obtained from the samples whether after reduction at 300°C the sample was either (a) cooled to room temperature under H_2 flow or (b) evacuated at 300°C and then cooled under vacuum. In a typical experiment, the sample was heated to the desired temperature in vacuum (10^{-3} mbar), exposed to H_2 (or 10% CO/He) flow of 100 cc/min for 30 min and cooled down to room temperature under flowing H_2 (or 10% CO/He). The introduction chamber was then evacuated to 10^{-3} mbar and the sample was forwarded to the analysis chamber. The characteristic photoemission peaks from Ce(*3d*), Rh(*3d*), O(*1s*), C(*1s*), and Cl(*2p*) core levels were recorded for each sample. Binding energies were corrected for charging by reference to adventitious carbon at 284.8 eV.

FTIR experiments. A Nicolet 740 FTIR spectrometer equipped with a DRIFT cell was used in the present study. The cell, containing ZnSe windows which are cooled by circulating water through blocks in thermal contact with the windows, allow *in situ* collection of spectra in the temperature range of 20–300°C, at atmospheric pressure. For all spectra, a 32-scan data acquisition was carried out at a resolution of 4.0 cm^{-1}. During measurements, external optics were purged with dry nitrogen in order to minimize the level of water vapor and carbon dioxide in the sample chamber. The sample used (ca 50 mg) was in finely powdered form and its surface was carefully flattened in order to increase the intensity of the IR beam by reflection. Before exposure to 1% CO (in Ar), the catalyst sample was heated in Ar to 300°C and then the feed was changed to H_2 for at least 1 h for reduction. The sample was subsequently exposed to Ar at the same temperature to purge H_2. The background spectra were collected at the desired temperatures before switching to CO. For studying the thermal stability of the adsorbed CO species, the Cl-free and Cl-containing Rh/CeO_2 catalysts were first exposed to CO at 200°C until equilibrium was reached. The samples were then cooled to room temperature in an atmosphere of CO, followed by purging with Ar for about 3 min. Finally, the temperature was stepwise increased under Ar flow, and IR spectra were recorded at desired temperatures.

3. RESULTS AND DISCUSSION

3.1. Catalyst Characterization

The surface elemental composition of the Cl-free and Cl-containing Rh/CeO_2 catalysts was measured by XPS and has been reported elsewhere (31). It was found that the Rh/CeO_2 catalyst prepared using $RhCl_3 \cdot H_2O$ as the metal precursor retains a significant amount of Cl species on the ceria surface (~7 at%) after reduction with hydrogen at 300°C, while a large amount of cerium (~30%, compared to 4% over Cl-free Rh/CeO_2) exists in the Ce^{3+} oxidation state, probably due to the formation of cerium oxychloride [$Ce^{(III)}OCl$] (31).

The XPS spectra obtained from the Cl-free Rh/CeO_2 catalyst in the Rh(*3d*) region are presented in Figs. 1a–c. The spectrum obtained following *in situ* reduction of the Rh/CeO_2(N) sample with hydrogen at 300°C is shown in Fig. 1a. Four peaks can be distinguished in this spectrum, which can be attributed to two sets of Rh(*3d*) peaks arising from two different oxidation states of rhodium: the bands at 306.8 and 311.6 eV originate from one state and the bands

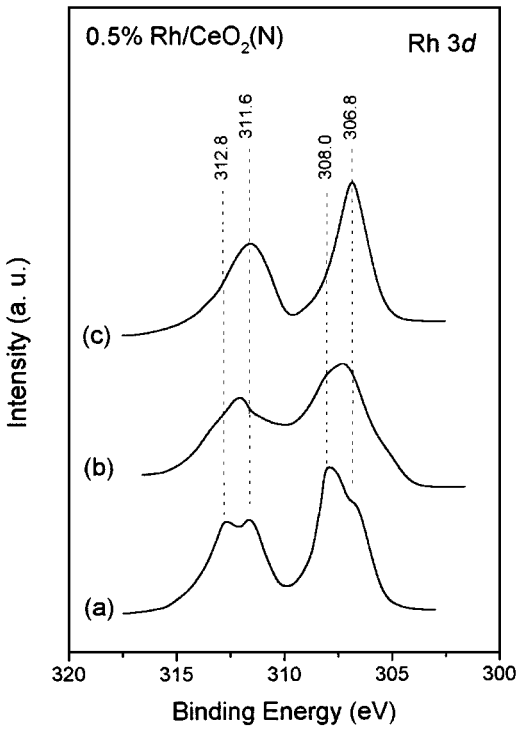

FIG. 1. Rh(*3d*) XPS spectra of 0.5% $Rh/CeO_2(N)$ catalyst obtained (a) after H_2 reduction at 300°C, (b) after CO adsorption at 25°C for 30 min, (c) after CO adsorption at 300°C for 30 min.

at 308.0 and 312.8 eV from the other. For rhodium metal foil, the Rh-$3d_{5/2}$ and -$3d_{3/2}$ photoemission peaks appear at 307.0 and 311.8 eV, respectively (32). The doublet at 306.8 and 311.6 eV (Fig. 1a) can then be attributed to Rh^0 species. The peaks located at 308.0 and 312.8 eV (Fig. 1a) occur at about 1.2 eV above the binding energy corresponding to Rh^0 and can be attributed to Rh^+ species (16, 18). It is clear that treatment of the $Rh/CeO_2(N)$ catalyst in hydrogen at 300°C under the experimental conditions employed is not adequate to completely reduce the rhodium particles (Fig. 1a). This is in accordance with the results of other investigators who have reported similar behavior studying reduction of rhodium supported on various materials at comparable temperatures (15, 16, 18).

The XPS spectrum obtained from the $Rh/CeO_2(N)$ sample following exposure to a 10% CO/He mixture at 25°C for 30 min is shown in Fig. 1b. Two broad bands are observed which may be attributed, as in the case of spectrum 1a, to the convolution of two doublets of peaks arising from the existence of Rh^0 and Rh^+ species. There appears to be, however, a small change in the relative population of the Rh^0 and Rh^+ species, as can be seen by comparison of the spectra obtained prior to and after CO adsorption (Figs. 1a, b). It is observed that CO adsorption at 25°C results in a relative increase of the population of Rh^+, as indicated by the decrease in the resolution between the Rh($3d_{5/2}$) and (Rh$3d_{3/2}$) peaks (Fig. 1b). This implies that CO adsorption at room temperature favors oxidation of Rh^0 to Rh^+.

When CO adsorption occurs at 300°C (Fig. 1c), the bands due to the Rh^0 particles are the dominant peaks in the Rh(*3d*) photoemission spectrum. It is observed that this treatment leads to almost complete reduction of Rh^+ to Rh^0. Although the bands due to Rh^+ cannot be clearly distinguished, a small portion of rhodium may still exist in the Rh^+ oxidation state as can be deduced from the FWHM of the peaks which is about 2.2 eV (Fig. 1c), compared to 1.6 eV observed for the rhodium foil (32).

From the spectra presented in Fig. 1, it becomes evident that treatment of $Rh/CeO_2(N)$ with CO at room temperature results in oxidation of an amount of Rh^0 to Rh^+ (Fig. 1b), while, at 300°C, the same treatment leads to reduction of rhodium particles (Fig. 1c). This behavior is in accordance with the XPS results of Buchanan *et al.* (19) who studied the oxidation state of Rh supported on TiO_2 as a function of oxidation and reduction temperature. The authors found that carbon monoxide exposure induces oxidative disruption of metallic Rh clusters at temperatures as low as −110°C, while at temperatures above 200°C, CO exposure leads to reduction of oxidized rhodium. Similar results have been obtained from rhodium supported on $TiO_2(110)$ (20) and Al_2O_3 (16).

It is interesting to note that CO is a better reducing agent than H_2 for rhodium, under the experimental conditions employed here: Treatment in CO at 300°C leads to almost complete reduction to Rh^0 (Fig. 1c), while treatment in hydrogen at the same temperature leads to the formation of both Rh^0 and Rh^+ species (Fig. 1a). This is probably due to the formation of large amounts of hydroxyl groups on the ceria surface upon treatment of $Rh/CeO_2(N)$ catalysts with hydrogen (31), which may stabilize rhodium in the Rh^+ oxidation state.

The corresponding spectra obtained from the Cl-containing sample are presented in Figs. 2a–c. The spectrum obtained following reduction with hydrogen at 300°C for 30 min is shown in Fig. 2a. Two broad peaks located at about 307.3 and 312.3 eV are clearly observed, which may again be attributed to the existence of rhodium particles in both the Rh^0 and Rh^+ oxidation states. These species were also present over the $Rh/CeO_2(N)$ sample (Fig. 1a). It is observed that treatment of $Rh/CeO_2(Cl)$ with hydrogen at 300°C is inadequate to completely reduce rhodium particles, as in the case of the Cl-free sample. In addition to the doublets due to Rh^0 and Rh^+ species, two weak bands, appearing at 310.3 (shoulder) and 315.1 eV can also be distinguished. This doublet, which is not observed over the Cl-free sample, can be attributed to the existence of rhodium particles in a higher oxidation state: The binding energy of Rh^{3+} in as-prepared catalysts derived from $RhCl_3 \cdot 3H_2O$ appears in the range of 310.2–310.7 eV (16, 33, 34) while the mean value of the Rh($3d_{5/2}$) binding energy of rhodium

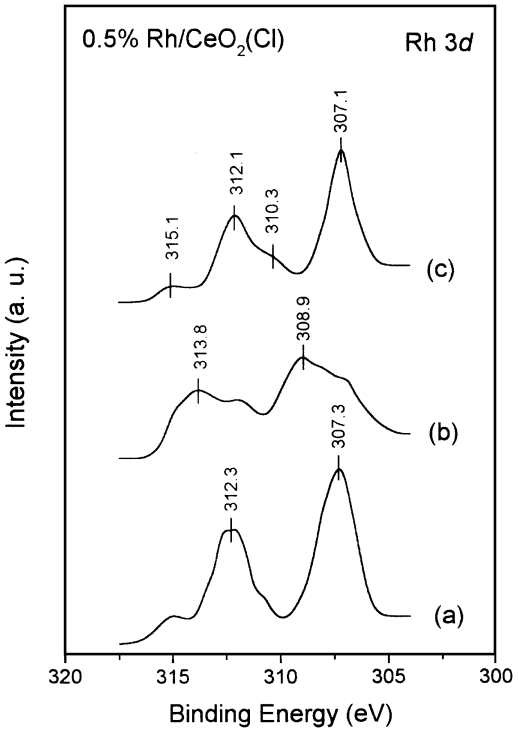

FIG. 2. Rh(*3d*) XPS spectra of 0.5% $Rh/CeO_2(Cl)$ catalyst obtained (a) after H_2 reduction at 300°C, (b) after CO adsorption at 25°C for 30 min, (c) after CO adsorption at 300°C for 30 min.

in Rh^{3+}-containing compounds is 310.3 eV (18). It is then reasonable to suggest that the doublet observed at 310.3 and 315.1 eV (Fig. 2a) is due to a Rh^{3+} species. XPS results of the present study (not shown) indicate that chlorine is present on the $Rh/CeO_2(Cl)$ surface under all experimental conditions reported here. It can then be deduced that the presence of Rh^{3+} species is associated with residual chlorine of the support, originating from the catalyst preparation method.

When the hydrogen-treated $Rh/CeO_2(Cl)$ sample was exposed to CO at 25°C for 30 min, the spectrum shown in Fig. 2b was obtained. This complex spectrum is due to the convolution of peaks associated with the presence of Rh^0, Rh^+, and Rh^{3+} species, as described above. It is observed that the peaks due to Rh^0 are significantly lowered in intensity, while those ascribed to Rh^+ are now clearly resolved. The Rh^{3+} doublet cannot be distinguished due to overlapping with the much more intense bands of Rh^+. It is evident that exposure of the $Rh/CeO_2(Cl)$ sample to CO at room temperature results in oxidation of a significant portion of the reduced Rh^0 species, indicating that the presence of chlorine strongly favors the formation of Rh^+ upon interaction of rhodium with CO at room temperature. As a result, the surface of the Cl-containing catalyst contains significant amounts of Rh^0, Rh^+, and Rh^{3+} species under the present experimental conditions.

The spectrum shown in Fig. 2c was obtained following CO adsorption on $Rh/CeO_2(Cl)$ at 300°C, for 30 min. As in the case of the Cl-free sample (Fig. 1c), a significant amount of the rhodium particles is reduced to Rh^0, while small amounts of Rh^+ are possibly still present on the surface. It is interesting to notice that the doublet attributed to Rh^{3+} species (310.3 and 315.1 eV) is still clearly observable, indicating that treatment with CO at 300°C does not result in the reduction of this species. The failure to completely reduce Rh^{3+} with CO at elevated temperatures provides additional evidence that this species is most probably stabilized by the Cl-containing support. This is in accordance with the work of Johnston *et al.* (14) who found evidence that γ-Al_2O_3-supported rhodium particles may be bonded to residual chlorine and proposed that the presence of chlorine ions may be necessary to stabilize Rh^+ entities.

Considering the role of chlorine in forming and/or stabilizing Rh^+ and Rh^{3+} species on $Rh/CeO_2(Cl)$ catalysts, the following arguments can be made: The formation of Rh^+ sites is usually attributed to oxidation of Rh^0 by hydroxyl groups present on the surface of the support and/or to the dissociation of CO followed by oxidation of Rh^0 with the adsorbed oxygen (12, 27–29). In a previous study (31) it was shown by XPS and TPD-MS experiments that hydroxyl groups are not present on the Cl-containing $Rh/CeO_2(Cl)$ surfaces after reduction in hydrogen at 300°C. However, if the rhodium particles are associated with chlorine species of the support, then the latter can be the charged counterparts of the oxidized rhodium ions. It is then reasonable to suggest that, as in the case of the hydroxyl groups, chlorine may play the role of the intimate ion pair of the oxidized rhodium particles.

It should be noted here that UHV treatment in an XPS chamber could possibly lead to some surface redox chemistry (i.e., ceria reduction, Rh oxidation). However, our results indicate that such phenomena are not responsible for the observed Rh^+ and Rh^{3+} photoemission peaks. For example, no peaks due to oxidized Rh appear following treatment of $Rh/CeO_2(N)$ with H_2 at 500°C (not shown), indicating that UHV treatment does not result in measurable redox phenomena under the experimental conditions employed here.

3.2. FTIR Experiments

CO chemisorption over the Cl-containing and Cl-free Rh/CeO_2 catalysts was studied at adsorption temperatures of 25 and 200°C, employing FT-IR spectroscopy. Thermal desorption experiments were also conducted following equilibrium CO adsorption at 200°C to identify the nature of the thermally stable CO species.

3.2.1. CO chemisorption on $Rh/CeO_2(Cl)$. The FTIR spectra obtained following CO chemisorption on the $Rh/CeO_2(Cl)$ catalyst at room temperature are shown in Fig. 3.

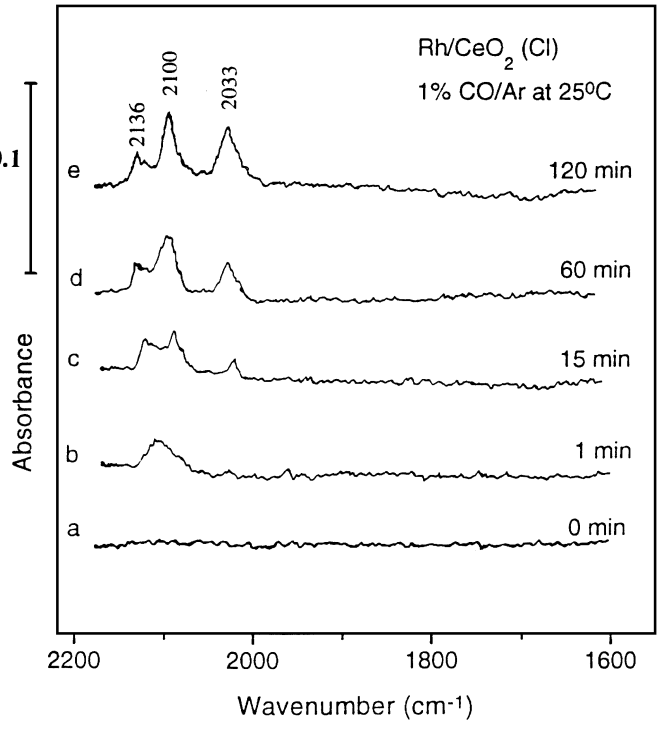

FIG. 3. FTIR spectra obtained from the reduced 0.5% $Rh/CeO_2(Cl)$ catalyst at 25°C (a) before exposure to CO, and after exposure to 1% CO/Ar mixture for (b) 1 min, (c) 15 min, (d) 60 min, (e) 120 min.

Following exposure of the reduced sample (Fig. 3a) to an 1% CO/Ar mixture for 1 min, only a small, broad band is detected above 2100 cm^{-1} (Fig. 3b). As time of exposure increases to 15 min, three bands, located at about 2136, 2100, and 2033 cm^{-1}, become clearly detectable (Fig. 3c). Prolonged exposure to CO, up to 2 h, does not result in any significant change in the band at 2136 cm^{-1}. However, the twin bands observed at 2100 and 2033 cm^{-1} develop continuously during the 2-h period and become the dominant bands observed in the region of 1880–2180 cm^{-1} (Figs. 3d,e). The twin bands at 2100 and 2033 cm^{-1} are attributed to the symmetric and antisymmetric stretching mode, respectively, of a Rh^+-gem-dicarbonyl [$Rh^+(CO)_2$] species (22). The band at 2136 cm^{-1} is not usually observed over reduced rhodium catalysts and is located in the spectral region, where CO/Rh^{3+} species are expected to absorb (22, 23). As will be shown later, this band is not observed over Cl-free Rh/CeO_2 catalysts and, therefore, is attributed to a CO species adsorbed on rhodium bound to chlorine. Although it is not possible to obtain straightforward evidence concerning the coordination environment of the CO species adsorbed on the Rh^{3+}, in the sequel we will refer to this species as $Rh^{3+}Cl_3(CO)$ to indicate that Rh^{3+} is associated to residual chlorine of the support. It should be mentioned here that high frequency IR bands in the region of 2122 to 2131 cm^{-1} have also been reported by Jin *et al.* (35) and Primet *et al.* (36, 37) following CO adsorption on pre-oxidized Pt/CeO_2 and Pt/Al_2O_3 catalysts, respectively, and were assigned to CO adsorbed on metal atoms either bound to oxygen or bound to partially oxidized metal clusters. In the present work, the presence of Rh–O species remaining on the catalyst should be excluded since before exposure to CO the sample was treated with hydrogen at 300°C for 1 h. Supporting evidence for the assignment of the 2100 and 2033 cm^{-1} bands to CO species adsorbed on Rh^+ and of the 2136 cm^{-1} band to CO species adsorbed on Rh^{3+} is given by the XPS measurements of the present study (Fig. 2) where it is clear that rhodium species in these oxidation states exist over $Rh/CeO_2(Cl)$ catalysts following CO adsorption at room temperature.

There are certain features of interest concerning the relative population and kinetics of adsorption of CO on $Rh/CeO_2(Cl)$: As observed in Fig. 3, the CO band at 2136 cm^{-1}, associated to CO adsorbed on Rh^{3+} sites, reaches its maximum intensity very fast following exposure to CO at room temperature, while the twin bands at 2100 and 2033 cm^{-1} due to the gem-dicarbonyl species on Rh^+ sites continue to develop with time-on-stream for 120 min (Fig. 3e). It is interesting to notice that no bands due to CO adsorption on Rh^0 sites are observed in these spectra, as also happens in the case of low metal-loaded, well dispersed catalysts, where only gem-dicarbonyl is observed, due to the existence of well-isolated rhodium particles on the support (22). This should not be the case here since the XPS experiments show that a significant amount of Rh^0 sites exist on the $Rh/CeO_2(Cl)$ catalyst following adsorption of CO at room temperature (Fig. 2b).

To further investigate these phenomena, CO chemisorption on the $Rh/CeO_2(Cl)$ catalyst was also conducted at an elevated temperature of 200°C, since increasing adsorption temperature can kinetically favor CO chemisorption. The spectra obtained following CO chemisorption on $Rh/CeO_2(Cl)$ at 200°C are shown in Figs. 4a–f. After exposure to the 1% CO/Ar mixture at 200°C for 5 min, only the band at 2136 cm^{-1} due to the $Rh^{3+}Cl_3(CO)$ species is observed (Fig. 4b), which further increases in intensity during 10 min on stream (Fig. 4c). Three more bands appear in the spectral region of 2000 to 2100 cm^{-1}, after 15 min on stream, located at 2038, 2070, and 2100 cm^{-1} (Fig. 4d). The bands at 2038 and 2100 cm^{-1} are due to the Rh^+-gem-dicarbonyl species which was also observed following CO adsorption at room temperature (Fig. 3). The band at 2070 cm^{-1}, which was not observed in Fig. 3, can be attributed to linearly bonded CO on Rh^0 sites (21, 22). Finally, after prolonged exposure to CO, two broad bands at around 1880 and 1930 cm^{-1} gradually develop. These bands can be attributed to two types of bridge-bonded CO on Rh^0 sites (21, 22).

As observed in Fig. 4, interconversions between the surface species occur after prolonged exposure of $Rh/CeO_2(Cl)$ to CO at 200°C. The intensity of the band at 2136 cm^{-1}, attributed to CO adsorption on Rh^{3+} sites,

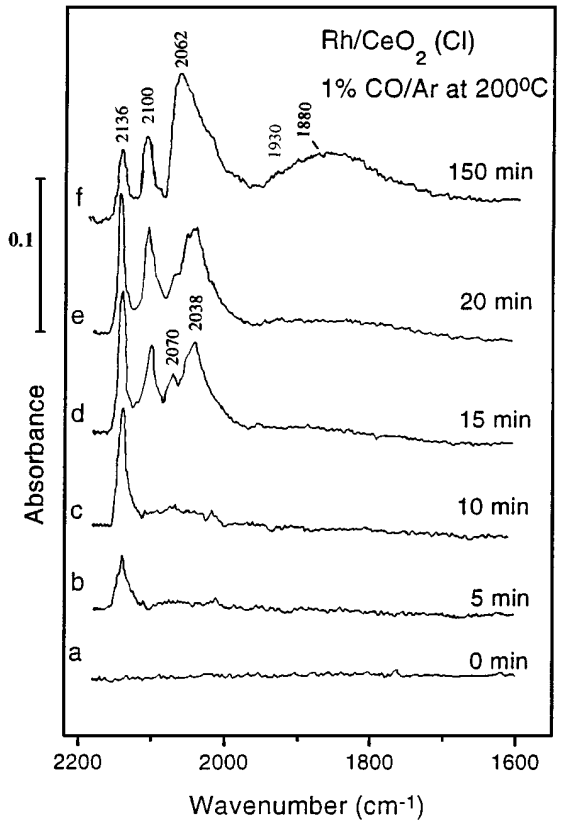

FIG. 4. FTIR spectra obtained from the reduced 0.5% $Rh/CeO_2(Cl)$ catalyst at 200°C (a) before exposure to CO, and after exposure to 1% CO/Ar mixture for (b) 5 min, (c) 10 min, (d) 15 min, (e) 20 min, (f) 150 min.

reaches a maximum after about 10 min on stream (Fig. 4c) and tends to be relatively stable. Only after this occurs, the twin bands at 2100 and 2038 cm^{-1} start developing at a significant rate, followed by the bands at around 2070, 1930, and 1880 cm^{-1}. The band at 2038 cm^{-1} becomes broadened and shifts to higher frequencies, due to overlapping with the band at 2070 cm^{-1} (Fig. 4e). After more than 20 min on stream, the intensity of the band at 2136 cm^{-1} is reduced significantly, indicating that a portion of the corresponding rhodium species is reduced by CO (Fig. 4f). Although the band at 2100 cm^{-1} does not change significantly in intensity for times of exposure longer than 15 min, the linearly adsorbed CO band at 2070 cm^{-1} develops continuously during this period (Figs. 4d–f). The latter band also gradually shifts to lower frequencies as a result of overlapping with the gem-dicarbonyl band at ca 2038 cm^{-1}. Apparently, the development of the linearly adsorbed CO band partly occurs at the expense of the band at 2136 cm^{-1}, i.e. a portion of Rh^{3+} sites are reduced to Rh^0 sites. Equilibrium of CO chemisorption at 200°C on the different rhodium sites is finally reached after more than 2 h of exposure to 1% CO/Ar mixture (Fig. 4f). The most intense bands are now the linearly and bridged adsorbed CO on the Rh^0 sites at around 2062 and 1880 cm^{-1}, respectively. The intensity of the band at 2136 cm^{-1} is still significant, implying that a considerable amount of Rh^{3+} species still remains on the surface and cannot be removed by CO under the conditions of the present experiment. This has also been verified with the XPS experiments (Fig. 2).

From the FTIR spectra presented in Figs. 3 and 4, it may be concluded that the coordination of CO on the $Rh^{3+}Cl_3$ sites results in suppression of CO chemisorption on Rh^0 sites and in retardation of the rate of CO chemisorption to reach equilibrium. It seems that such kind of poisoning effect is not due to geometric blocking but due to a long-distance electronic interaction. When all the $Rh^{3+}Cl_3$ sites have been saturated with CO, i.e. forming the $Rh^{3+}Cl_3(CO)$ species, such kinds of long distance electronic interactions disappear, permitting the occurrence of CO chemisorption on Rh^0 sites.

3.2.2. CO chemisorption on $Rh/CeO_2(N)$. In order to better evaluate the effect of residual chlorine on the interaction of CO with Rh dispersed on CeO_2, the chemisorption of CO on the $Rh/CeO_2(N)$ catalyst, which is free of Cl species, was also studied. Since numerous studies have already been reported (3–5, 9, 38–40) on CO chemisorption on Rh/CeO_2 at room temperature, only CO adsorption on the $Rh/CeO_2(N)$ at 200°C is presented here to facilitate comparison with the preceding results.

The spectra obtained following CO chemisorption on the $Rh/CeO_2(N)$ catalyst at 200°C are shown in Figs. 5a–d. At

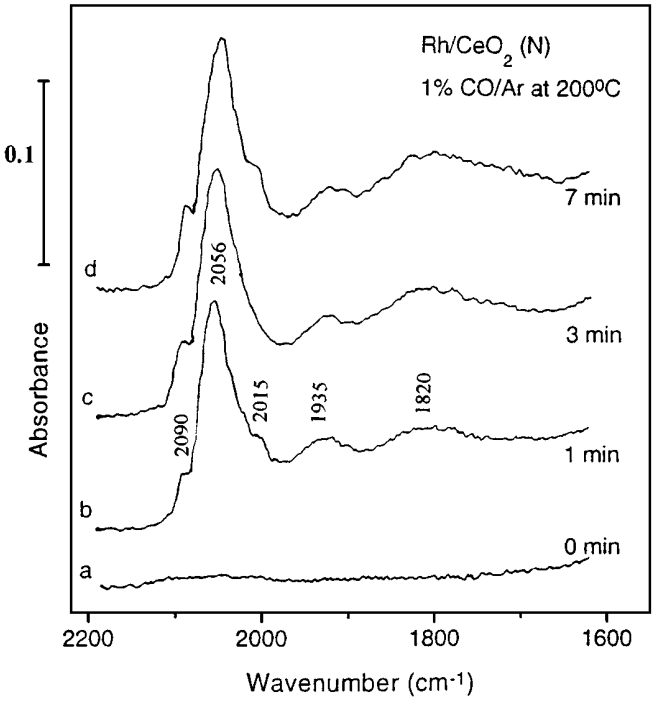

FIG. 5. FTIR spectra obtained from the reduced 0.5% $Rh/CeO_2(N)$ catalyst at 200°C (a) before exposure to CO, and after exposure to 1% CO/Ar mixture for (b) 1 min, (c) 3 min, (d) 7 min.

least three well-separated bands at 2056, 1935, 1820 cm^{-1}, and two shoulder bands at 2090 and 2015 cm^{-1} are observed after exposing the sample to 1% CO/Ar mixture for 1 min (Fig. 5b). Increasing exposure time results only in a small increase in the intensity of all bands. After approximately 7 min on stream, all bands tend to be stable, indicating that CO chemisorption has reached equilibrium (Fig. 5d). The intense band at 2056 cm^{-1} corresponds to linearly adsorbed CO on Rh^0 sites, while the two bands at 1935 and 1820 cm^{-1} are due to two types of bridged CO on Rh^0 sites. The two shoulder bands at ca 2090 and 2015 cm^{-1} are assigned to gem-dicarbonyl species. It is observed that the adsorbed CO species on Rh^0 sites are dominant, while the gem-dicarbonyl species are only minor.

Previous studies of CO chemisorption on reduced rhodium catalysts show that CO chemisorption is a fairly fast process and that the appearance of gem-dicarbonyl bands usually takes place after those of linearly and bridge-bonded CO on Rh^0 (12, 25, 27, 28). This seems to be the case for the $Rh/CeO_2(N)$ catalyst as well, as observed in Fig. 5. Adsorption of CO on the rhodium particles reaches equilibrium very fast (Figs. 5a–d) with the formation of linear-bonded CO on Rh^0 sites (2056 cm^{-1}), bridge-bonded CO on Rh^0 (1935 and 1820 cm^{-1}), and gem-dicarbonyl species on Rh^+ sites (twin bands at 2015 and 2090 cm^{-1}).

Comparing the spectra of Fig. 5 with the corresponding ones obtained from the $Rh/CeO_2(Cl)$ sample at the same adsorption temperature (Fig. 4), it becomes evident that the presence of Cl species significantly retards the rate of CO chemisorption and suppresses CO chemisorption on Rh^0 sites. Only when the Rh^{3+} sites have been saturated with CO, as indicated by reaching the maximum intensity of the $Rh^{3+}Cl_3(CO)$ band at 2136 cm^{-1} (Fig. 4), do the other types of chemisorbing sites start to adsorb CO, e.g. forming linearly adsorbed CO, bridged adsorbed CO, and gem-dicarbonyl species. It seems that the Cl species have little or no influence on CO chemisorption on localized chemisorbing sites, e.g. $Rh^{3+}Cl_3(CO)$ and $Rh^+(CO)_2$ which are characterized by the feature that the band position is invariable upon altering surface concentration (Figs. 3 and 4). Apparently, the presence of Cl species increases the relative population of the Rh^+-gem-dicarbonyl species among the surface CO species. This could be understood in either of two ways: (i) the presence of Cl species promote the formation of the gem-dicarbonyl species or (ii) they retard the formation of CO species on Rh^0 sites, both of which lead to a net result of enhanced relative population of the gem-dicarbonyl species. The results of the present study indicate that both of these routes are operable. The XPS spectra clearly show that the presence of chlorine favors the oxidative disruption of Rh–Rh bond upon CO chemisorption on the Rh^0 sites (Fig. 2), while the FTIR spectra presented in Figs. 3 and 4 show that CO adsorption on Rh^0 is retarded on Cl-containing Rh/CeO_2 catalysts.

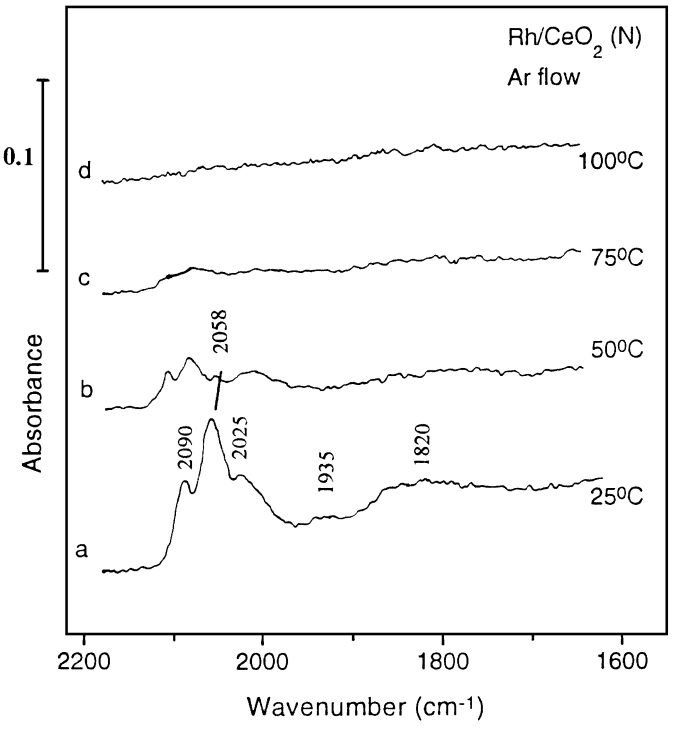

FIG. 6. FTIR spectra of CO adsorbed on the 0.5% $Rh/CeO_2(N)$ catalyst obtained following equilibrium chemisorption at 200°C, cooling down to room temperature under 1% CO/Ar mixture and subsequent heating in Ar flow to: (a) 25°C, (b) 50°C, (c) 75°C, (d) 100°C.

3.2.3. Desorption of CO from $Rh/CeO_2(N)$ and Rh/CeO_2 (Cl) catalysts. The spectra obtained from the $Rh/CeO_2(N)$ catalyst, following CO adsorption at 200°C, upon increasing temperature under Ar flow are shown in Figs. 6a–d. Five bands due to the adsorbed CO species, at 2090, 2058, 2025, 1935, and 1820 cm^{-1}, are observed at room temperature (Fig. 6a). The intensity of all five bands is reduced significantly as the temperature is increased to 50°C (Fig. 6b). When the temperature is further increased to 75°C, the intensities of all bands become very weak (Fig. 6c). Finally, all CO species are completely removed from the surface upon heating the sample to 100°C (Fig. 6d).

The corresponding spectra obtained from the $Rh/CeO_2(Cl)$ catalyst are shown in Figs. 7a–f. At least six bands, located at 2136, 2100, 2066, 2038, 1960, and 1890 cm^{-1} are observed at room temperature (Fig. 7a). Comparing with the corresponding spectrum of the $Rh/CeO_2(N)$ sample (Fig. 6a), it is again observed that the $Rh/CeO_2(Cl)$ sample has similar surface CO species, plus an additional one responsible for the absorption band at 2136 cm^{-1}. The intensity of the five bands at 2100, 2066, 2038, 1960, and 1890 cm^{-1} is somewhat reduced as temperature is increased to 75°C (Fig. 7c). These bands are completely removed upon reaching 100°C, indicating that the Rh^+-gem dicarbonyl species, and the linearly and bridged adsorbed CO on Rh^0 sites have approximately the same order of thermal stability,

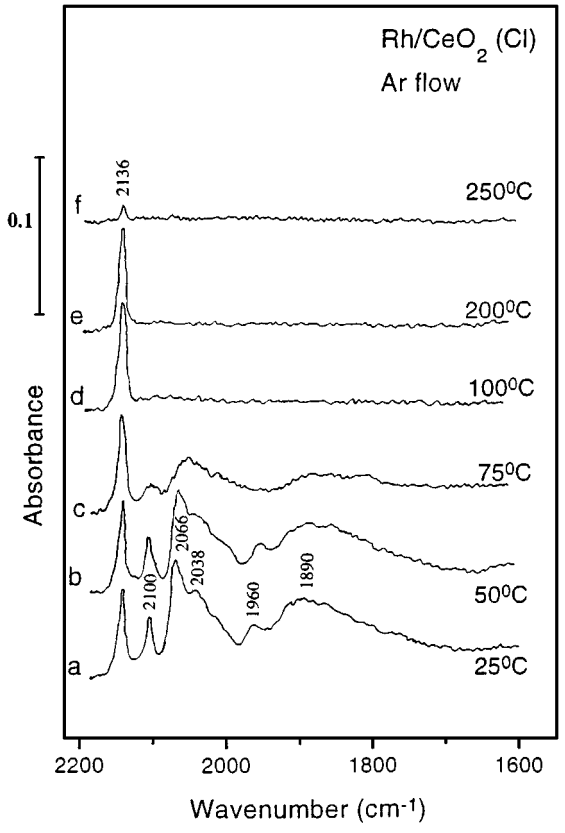

FIG. 7. FTIR spectra of CO adsorbed on the 0.5% Rh/CeO_2(Cl) catalyst obtained following equilibrium chemisorption at 200°C, cooling down to room temperature under 1% CO/Ar mixture and subsequent heating in Ar flow to: (a) 25°C, (b) 50°C, (c) 75°C, (d) 100°C, (e) 200°C, (f) 250°C.

desorbing from the Rh/CeO_2(Cl) surface in the temperature range between 50–100°C, under the experimental conditions employed. This behavior is generally similar to that observed over the Rh/CeO_2(N) catalyst (Fig. 6). The most striking feature observed in Fig. 7 is the unusually high thermal stability of the band at 2136 cm^{-1}. While the other five bands disappear completely at temperatures below 100°C, the 2136 cm^{-1} band does not show any reduction in intensity at temperatures up to 200°C. Only after heating to 250°C, the intensity of this band is reduced significantly (Fig. 7f). This is in accordance with the results of our previous study in which a thermally stable CO species was observed to desorb from the Rh/CeO_2(Cl) catalyst at approximately 300°C in TPD-MS experiments (31). This TPD peak was only observed over the Cl-containing sample.

At present, it is unclear why CO is bound so strongly on the Rh^{3+} sites. From the fact that this band is very sharp and that the band position does not change upon altering the concentration of the species, it can be derived that CO is locally bound to one atomic Rh^{3+} site. If there is no involvement of other ligands (e.g., Cl species), CO is unlikely to be bound on Rh^{3+} sites so strongly. It is interesting to note that the $Rh^{3+}Cl_3(CO)$ species is the first one formed upon CO chemisorption, and it is also the last one desorbing from the surface upon heating.

The high thermal stability of the $Rh^{3+}Cl_3(CO)$ species absorbing at 2136 cm^{-1} is rather unexpected, compared to the lower thermal stability of the other species which absorb at lower frequencies, since it is reasonable to expect that the stronger the bond between the carbon and oxygen atom, the weaker the bond between the carbon and the metal atoms. This "unusual" behavior has been frequently observed and is explained by taking into account the competition between the desorption process and the possible surface reactions which may take place during the temperature programmed desorption (38–40). For example, it is not straightforward from the TPD-FTIR spectra shown in Figs. 6 and 7 to conclude if the disappearance of the IR bands is due to desorption or reaction of the various CO species. In a previous TPD-MS study of the present catalysts, it was found that large amounts of CO_2 are produced upon heating, due to the reaction of the adsorbed CO species with oxygen originating from ceria. The high thermal stability of the $Rh^{3+}Cl_3(CO)$ species can then be attributed to its higher resistance to oxidation, compared to the other adsorbed CO species, which readily become oxidized.

4. SUMMARY AND CONCLUSIONS

The presence of residual Cl species on the Rh/CeO_2 catalyst imposes significant changes in the CO adsorption/desorption behavior and the oxidation state of supported rhodium. Over the Cl-containing sample, a significant amount of rhodium particles exists in the Rh^{3+} oxidation state, in addition to Rh^0 and Rh^+, which is not reduced even following treatment with H_2 or CO at 300°C.

Several striking features in the processes of CO adsorption and desorption on Rh/CeO_2, related to the presence of Cl species are also observed which are summarized below:

1. The presence of Cl species on the Rh/CeO_2 surface greatly retards the kinetic rate of CO chemisorption on rhodium.

2. The selectivity of CO adsorption towards different types of chemisorbed sites is remarkably altered due to the presence of Cl species which inhibit CO chemisorption on Rh^0.

3. The first species which appears upon CO chemisorption on Rh/CeO_2(Cl) is $Rh^{3+}Cl_3(CO)$, followed by the Rh^+-gem-dicarbonyl species. Only when all the $Rh^{3+}Cl_3$ sites have been saturated with CO, does CO chemisorption on Rh^0 sites occur.

4. The relative population of the various adsorbed CO species at equilibrium is affected by the presence of Cl species. While the linearly and bridged CO species adsorbed on Rh^0 are the dominant ones on the Cl-free Rh/CeO_2(N) surface, significant amounts of $Rh^{3+}Cl_3(CO)$ and

$Rh^{+}(CO)_2$ species coexist with the linearly and bridged adsorbed CO on the Rh^0 sites on the $Rh/CeO_2(Cl)$ surface.

5. The thermal stability of the Rh^{+}-gem dicarbonyl species, and of the linearly and bridged adsorbed CO on Rh^0 sites is of the same order. All these species desorb from the surface in the temperature range of 50–100°C, regardless of the presence or not of Cl species on the surface. The $Rh^{3+}Cl_3(CO)$ species has a uniquely high thermal stability, as compared to the other species, and can be retained on the surface at temperatures up to about 200°C.

ACKNOWLEDGMENT

The authors thank Dr. S. Neophytides of the Institute of Chemical Engineering and High Temperature Chemical Processes (ICE/HT) for his kind assistance with the XPS measurements.

REFERENCES

1. Trovarelli, A., *Catal. Rev. Sci. Eng.* **38**, 439 (1996).
2. Engler, B., Koberstein, E., and Schubert, P., *Appl. Catal.* **48**, 71 (1989).
3. Trovarelli, A., de Leitenburg, C., and Dolcetti, G. J., *Chem. Soc. Chem. Commun.*, 472 (1991).
4. Trovarelli, A., Dolcetti, G., de Leitenburg, C., Kaspar, J., Finetti, P., and Santoni, A., *J. Chem. Soc. Faraday Trans.* **88**, 1311 (1992).
5. De Leitenburg, C., and Trovarelli, A., *J. Catal.* **156**, 171 (1995).
6. Le Normand, F., Hilaire, L., Kili, K., Krill, G., and Maire, G., *J. Phys. Chem.* **92**, 2561 (1988).
7. Le Normand, F., Barrault, J., Breault, R., Hilaire, L., and Kiennemann, A., *J. Phys. Chem.* **95**, 257 (1991).
8. Kepinski, L., Wolcyrz, M., and Okal, J., *J. Chem. Soc. Faraday Trans.* **91**, 507 (1995).
9. Bernal, S., Botana, F. J., Calvino, J. J., Cauqui, M. A., Cifredo, G. A., Jobacho, A., Pintado, J. M., and Rodriguez-Izquierdo, J. M., *J. Phys. Chem.* **97**, 4118 (1993).
10. Badri, A., Binet, C., and Lavalley, J. C., *J. Phys. Chem.* **100**, 8363 (1996).
11. Kiennemann, A., Breault, R., Hindermann, J. P., and Laurin, M., *J. Chem. Soc. Faraday Trans.* **83**, 2119 (1987).
12. Van't Blik, H. F. J., Van Zon, J. B. A. D., Huizinga, T., Vis, J. C., Koningsberger, D. C., and Prins, R., *J. Phys. Chem.* **87**, 2264 (1983).
13. Van der Lee, G., Schuller, B., Post, H., Favre, T. L. F., and Ponec, V., *J. Catal.* **98**, 52 (1986).
14. Johnston, P., Joyner, R. W., Pudney, P. D. A., Shpiro, E. S., and Williams, B. P., *Faraday Disc. Chem. Soc.* **89**, 91 (1990).
15. Baltanas, M. A., Onuferko, J. H., McMillan, S. T., and Katzer, J. R., *J. Phys. Chem.* **91**, 3772 (1987).
16. Grunert, W., Wolf, D., Buyevskaya, O. V., Walter, K., and Baerns, M., *Z. Phy. Chem.* **197**, 49 (1996).
17. Belton, D. N., and Schmieg, S. J., *Surf. Sci.* **199**, 518 (1988).
18. Kawai, M., Uda, M., and Ichikawa, M., *J. Phys. Chem.* **89**, 1654 (1985).
19. Buchanan, D. A., Hernandez, M. E., Solymosi, F., and White, J. M., *J. Catal.* **125**, 456 (1990).
20. Evans, J., Hayden, B., Mosselmans, F., and Murray, A., *Surf. Sci.* **279**, L159 (1992).
21. Yang, A. C., and Garland, C. W., *J. Phys. Chem.* **61**, 1504 (1957).
22. Rice, C. A., Worley, S. D., Curtis, C. W., Guin, J. A., and Tarrer, A. R., *J. Chem. Phys.* **74**, 6487 (1981).
23. Trautmann, S., and Baerns, M., *J. Catal.* **150**, 335 (1994).
24. Solymosi, F., Pasztor, M., and Rakhely, G. T., *J. Catal.* **110**, 413 (1988).
25. Zhang, Z. L., Kladi, A., and Verykios, X. E., *J. Phys. Chem.* **98**, 6804 (1994).
26. Lavalley, J. C., Saussey, J., Lamotte, J., Breault, B., Hindermann, J. P., and Kiennemann, A., *J. Phys. Chem.* **94**, 5941 (1990).
27. Solymosi, F., and Pasztor, M., *J. Phys. Chem.* **89**, 4789 (1985).
28. Basu, P., Panayotov, D., and Yates, J. T., Jr., *J. Phys. Chem.* **91**, 3133 (1987).
29. Bergeret, G., Gallezot, P., Gelin, P., Ben Taarit, Y., Lefebvre, F., Naccache, C., and Shannon, R. D., *J. Catal.* **104**, 279 (1987).
30. Solymosi, F., and Knozinger, H., *J. Chem. Soc. Faraday Trans.* **86**, 389 (1990).
31. Kondarides, D. I., and Verykios, X. E., *J. Catal.*, in press.
32. "Practical Surface Analysis, Vol. 1. Auger and X-ray Photoelectron Spectroscopy" (D. Briggs and M. P. Seah, Eds.), Appendix 6., Wiley, New York, 1990.
33. Van't Blik, H. F. J., van Zon, J. B. A. D., Huizinga, J., Vis, J. C., Koningsberger, D. C., and Prins, R., *J. Am. Chem. Soc.* **107**, 3139 (1985).
34. Borg, H. J., van Oetelaar, L. C. A., and Niemantsverdriet, J. W., *Catal. Lett.* **17**, 81 (1993).
35. Jin, T., Zhou, Y., Mains, G. T., and White, J. M., *J. Phys. Chem.* **91**, 5931 (1987).
36. Primet, M., *J. Catal.* **88**, 273 (1984).
37. Primet, M., Basset, J. M., Mathieu, M. V., and Prettre, M., *J. Catal.* **29**, 213 (1973).
38. Bernal, B., Calvino, J. J., Cifredo, G. A., Rodriguez-Izquierdo, J. M., Perrichon, V., and Laachir, A., *J. Catal.* **137**, 1 (1992).
39. Bernal, S., Botana, F. J., Garcia, R., Kang, Z., Lopez, M. L., Pan, M., Ramirez, F., and Rodriguez-Izquierdo, J. M., *Catal. Today* **2**, 653 (1988).
40. Bernal, S., Calvino, J. J., Cifredo, G. A., Gatica, J. M., Omil, J. A. P., and Pintado, J. M., *J. Chem. Soc. Faraday Trans.* **89**, 3499 (1993).